

Full Length Research Paper

The flow of a Carreau fluid down an incline with a free surface

M. S. Tshehla

Department of Mathematics, Faculty of Military Science, University of Stellenbosch P/Bag X2, Saldanha, 7395, South Africa. E-mail: samuel@ma2.sun.ac.za.

Accepted 18 April, 2011

This paper deals with the effect of a Carreau fluid flow down an inclined plane with a free surface. The fluid film is thin, so that lubrication approximation may be applied. In general, the flow equations resulting from the variable viscosity model must be solved numerically. However, when the viscosity variation is small, then an asymptotic approximation is possible. The full solutions for the velocity and temperature profiles are derived using the fourth order Runge-Kutta numerical method. The flow controlling parameters such as the non-dimensional viscosity variation parameter, the Biot and the Brinkman numbers, are found to have a profound effect on the resulting flow profiles.

Key words: Lubrication theory, Carreau fluid, viscosity.

INTRODUCTION

In industrial systems, the hydrodynamics of fluid flow under gravity is of practical interest in many engineering applications such as coating processes (Makinde, 2006). It is a well known fact in fluid dynamics studies, that the property which is most sensitive to temperature rise is the viscosity (Bair, 2006; Makinde, 2010). The Carreau model has caught the attention of researchers and engineers. Bair (2006) and Myers (2005) studied the application of non-Newtonian models to thin film flow with a free surface. The results showed that the Carreau and Ellis models were compared favourably, while the power law model can produce inaccurate results for the velocity profiles. Fomin et al. (2003) investigated the shear rate dependent viscosity models using a numerical technique, and the results revealed that the Carreau and Ellis models, exhibit Newtonian behaviour near the free surface and power law behaviour near the wall of a rotating cylinder. Further, experimental analysis for the Carreau model is detailed in (Eastop et al., 1978; Feng et al., 1999; Haldenwang et al., 2004; Rouser et al., 2007) for polymer processing materials. In most of these references, the focus is on the application of shear rate viscosity models in experimental operations. In this paper, the Carreau model will be investigated for flow with a free surface and the velocity and temperature profiles are derived using an asymptotic approach and

numerical scheme is used to obtain the full solution. We extend the pioneering work by Myers (2005) to include the energy equation, to the equation governing the flow in order to solve for the temperature of the fluid. The main reason for using an asymptotic analysis so that we can clearly illustrate how the parameters affect the flow by looking into the dominant terms from the governing equations. This approach can be used to validate numerical methods.

PROBLEM FORMULATION

Figure 1 represents a two-dimensional laminar flow with a free surface. The figure depicts an infinitely wide channel of typical length scale L in the x direction and height H in the y direction. The fluid flows down a plane inclined at an angle β , and the dominant driving force for the flow is gravity, denoted g . The ambient temperature is denoted T_a the fluid temperature is denoted T and the temperature at the bottom surface is denoted T_s . The fluid viscosity is denoted μ .

In developing the mathematical model for the fluid flow, the following assumptions will be made:

- 1) The fluid is incompressible and the fluid viscosity

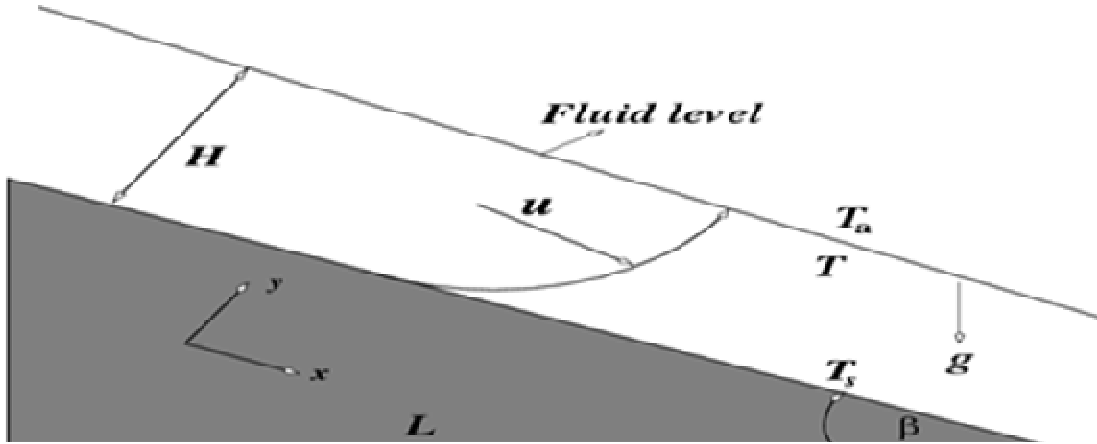


Figure 1. Free surface flow geometrical representation.

varies.

- 2) The governing equations are derived for a thin film flow such that lubrication theory may be applied.
- 3) The film height H is considered to be constant.
- 4) The flow regime is laminar.

Taking into account these assumptions, the continuity, Navier-Stokes and energy equations are written as follows:

$$\frac{\partial u}{\partial x} + \frac{\partial v}{\partial y} = 0, \tag{1}$$

$$\rho \left(\frac{\partial u}{\partial t} + u \frac{\partial u}{\partial x} + v \frac{\partial u}{\partial y} \right) = -\frac{\partial p}{\partial x} + \rho g \sin \beta + 2 \frac{\partial}{\partial x} \left(\mu \frac{\partial u}{\partial x} \right) + \frac{\partial}{\partial y} \left[\mu \left(\frac{\partial u}{\partial y} + \frac{\partial v}{\partial x} \right) \right], \tag{2}$$

$$\rho \left(\frac{\partial u}{\partial t} + u \frac{\partial v}{\partial x} + v \frac{\partial v}{\partial y} \right) = -\frac{\partial p}{\partial y} + \rho g \cos \beta + 2 \frac{\partial}{\partial y} \left(\mu \frac{\partial v}{\partial y} \right) + \frac{\partial}{\partial x} \left[\mu \left(\frac{\partial u}{\partial y} + \frac{\partial v}{\partial x} \right) \right], \tag{3}$$

$$\rho c_p \left(\frac{\partial T}{\partial t} + u \frac{\partial T}{\partial x} + v \frac{\partial T}{\partial y} \right) = k \left(\frac{\partial^2 T}{\partial x^2} + \frac{\partial^2 T}{\partial y^2} \right) + \left[\frac{\partial p}{\partial t} + u \frac{\partial p}{\partial x} + v \frac{\partial p}{\partial y} \right] + \mu \left[2 \left(\frac{\partial u}{\partial x} \right)^2 + \left(\frac{\partial u}{\partial x} + \frac{\partial v}{\partial y} \right)^2 + 2 \frac{\partial v}{\partial y} \frac{\partial u}{\partial x} \right], \tag{4}$$

where the notation is defined in Table 1. These governing equations are non-dimensionalised using the following scales:

$$x = Lx', \quad y = Hy', \quad u = Uu', \quad v = \frac{HU}{L}v', \quad t = \frac{L}{U}t', \quad \mu = \mu_0, \quad p = Pp' = \frac{\mu_0 UL}{H^2}p', \quad T = T_0 + (T_a - T_0)T' = T_0 + \Delta T T',$$

where all quantities with prime denote non-dimensional

parameters. The pressure scale $P = \mu_0 UL/H^2$ is standard for lubrication theory. The reference viscosity and the temperature difference are denoted by μ_0 and ΔT , respectively. To simplify notation, the primes are omitted from now on. Since the film is thin, the aspect ratio $\varepsilon = H/L \ll 1$. Using the scaled parameters Equations (1) to (4) now become:

$$\frac{\partial u}{\partial x} + \frac{\partial v}{\partial y} = 0. \tag{5}$$

$$\varepsilon^2 Re \left(\frac{\partial u}{\partial t} + u \frac{\partial u}{\partial x} + v \frac{\partial u}{\partial y} \right) = -\frac{\partial p}{\partial x} + 1 + 2\varepsilon^2 \frac{\partial}{\partial x} \left(\mu \frac{\partial u}{\partial x} \right) + \frac{\partial}{\partial y} \left[\mu \left(\frac{\partial u}{\partial y} + \varepsilon^2 \frac{\partial v}{\partial x} \right) \right]. \tag{6}$$

$$\varepsilon^2 Re^4 \left(\frac{\partial u}{\partial t} + u \frac{\partial v}{\partial x} + v \frac{\partial v}{\partial y} \right) = -\frac{\partial p}{\partial y} + \varepsilon \cot \beta + 2\varepsilon^2 \frac{\partial}{\partial y} \left(\mu \frac{\partial v}{\partial y} \right) + \varepsilon^2 \frac{\partial}{\partial x} \left[\mu \left(\frac{\partial u}{\partial y} + \varepsilon^2 \frac{\partial v}{\partial x} \right) \right]. \tag{7}$$

$$\varepsilon^2 Pe \left(\frac{\partial T}{\partial t} + u \frac{\partial T}{\partial x} + v \frac{\partial T}{\partial y} \right) = \varepsilon^2 \frac{\partial^2 T}{\partial x^2} + \frac{\partial^2 T}{\partial y^2} + Pr Ec \left[\frac{\partial p}{\partial t} + u \frac{\partial p}{\partial x} + v \frac{\partial p}{\partial y} \right] + \Phi, \tag{8}$$

where,

$$\Phi = Br \mu \left[2\varepsilon^2 \left(\frac{\partial u}{\partial x} \right)^2 + 2\varepsilon^2 \left(\frac{\partial v}{\partial y} \right)^2 + \left(\frac{\partial u}{\partial y} + \varepsilon^2 \frac{\partial v}{\partial x} \right)^2 \right]$$

The Péclet number $Pe = \rho c_p UL/\kappa$ represents the ratio of convective heat transport to the conductive heat transport and the Brinkman number $Br = \mu_0 U^2/\kappa \Delta T$ represents the ratio of heat dissipation to fluid conduction. The Prandtl number $Pr = \mu_0 c_p/\kappa$ denotes the ratio of diffusivity for momentum to thermal diffusivity. The Eckert number $Ec = U^2/c_p T_0$ denotes the ratio of kinetic energy to thermal mass. The velocity scale is given by $U = \rho g H^2 \sin \beta / \mu_0$, which denotes the ratio of gravitational

Table 1. Notation and typical units (Nomenclature).

Name	Symbol	Unit
$Bi = HK_c/\kappa$	Biot number	
$Br = \mu_0 U^2/k \Delta T$	Brinkman number	
C_p	Heat capacity	J. Kg ⁻¹ . K ⁻¹
$Ec = U^2/c_p T_0$	Eckert number	
g	Acceleration due to gravity	m s ²
H	Channel height	m
k	Thermal conductivity	W. m ⁻¹ . K ⁻¹
K_c	Heat transfer coefficient	W. m ⁻² . K ⁻¹
L	Channel length	m
P	Pressure scale	Pa
p	Pressure	Pa
$Pe = \rho c_p L U/k$	Péclet number	
$Pr = \mu_0 c_p/\kappa$	Prandtl number	
$Re = \rho U L/\mu_0$	Time	s
T	Temperature	°C
T_a	Ambient temperature	°C
T_s	Bottom surface temperature	°C
ΔT	Temperature drop	°C
$U = \rho g H^2 \sin \beta / \mu_0$	Velocity scale	m s ¹
(u, v)	Cartesian velocity	m s ¹
(x, y)	Cartesian coordinates	m
ε	Aspect ratio of the flow	
μ	Dynamic viscosity	kg. m ⁻¹ . s ⁻¹
μ_0	Dynamic viscosity reference	kg. m ⁻¹ . s ⁻¹
Φ	Viscous dissipation function	
ρ	Fluid density	kg. m ⁻³
θ	Coefficient of viscosity variation	K ⁻¹

forces to the dynamic viscosity. The parameter values may vary widely depending on the particular industrial application or the models under investigation. The parameter values for a lubricant are:

$$\mu_0 \sim 10^{-3} - 0.5 \text{ kg/ms}, \quad c_p \sim 2000 \text{ J/kgK}, \quad H \sim 10^{-3} \text{ m}, \\ k \sim 0.13 \text{ W/mK}, \quad K_c \sim 10^3, \quad L \sim 0.005, \quad \varepsilon \sim 10^{-4}, \quad \text{and} \\ \rho \sim 880 - 940 \text{ kg/m}^3.$$

The aforementioned experimental values listed are taken from several references, (Constantinescu, 1995; Holman, 1990; Khaled, 2008; Schetz, 1999, White, 1994). Using these values listed above we obtain:

$$Br = \mu_0 U^2/k \Delta T \sim 0.01 - 0.5, \quad Pe = \rho c_p UL/k \sim 10^5, \\ PrEc = \mu_0 U^2/kT_0 \sim 5 \times 10^{-4}, \quad Re = \rho UL/\mu_0 \sim 40 - 2000, \\ U = \rho g H^2 \sin 30/\mu_0 \sim 0.4 \text{ m/s}.$$

Despite the fact that the Péclet number is large, the

reduced Péclet number $\varepsilon^2 Pe \approx 10^{-3}$ is small and may be neglected in the governing equations. The reduced Reynolds number $\varepsilon^2 Re \approx 1.8 \times 10^{-5}$ may also be neglected. The reduced quantity $PrEc$ is also small, so it will be neglected from the governing equations. The Brinkman number may be close to unity and so must be retained. Using the aforementioned approximations Equations (5) to (8) may now be reduced to their final form:

$$\frac{\partial u}{\partial x} + \frac{\partial v}{\partial y} = 0. \quad (9)$$

$$-\frac{\partial p}{\partial x} + \frac{\partial}{\partial y} \left[\mu \left(\frac{\partial u}{\partial y} \right) \right] + 1 = 0 + \mathcal{O}(\varepsilon^2, \varepsilon^2 Re). \quad (10)$$

$$-\frac{\partial p}{\partial y} + \varepsilon \cot \beta = 0 + \mathcal{O}(\varepsilon^2, \varepsilon^4 Re). \quad (11)$$

$$\frac{\partial^2 T}{\partial y^2} + \mu Br \left(\frac{\partial u}{\partial y} \right)^2 = 0 + \mathcal{O}(\varepsilon^2, \varepsilon^2 Pe). \quad (12)$$

The velocity and the temperature profiles may be

determined after the boundary conditions associated with Equations (9) to (12) are stated.

Boundary conditions

1) At $y = 0$ a no slip boundary condition is applied and the temperature at the bottom surface is constant,

$$u(0) = v(0) = 0, \quad T(0) = 0. \quad (13)$$

2) At the free surface, the shear stress is zero and the fluid temperature is imposed by the air and substrate respectively,

$$\left(\frac{\partial u}{\partial y}\right)\Big|_{y=h} = 0, \quad \left(\frac{\partial T}{\partial y}\right)\Big|_{y=h} = Bi(T - 1), \quad (14)$$

where $Bi = HK_c/k$ is the Biot number and denotes the ratio of heat transfer to thermal conductivity Alhama et al. (2007) and Makinde (2006) The parameters k and K_c denote the thermal conductivity and heat transfer coefficient respectively. The fluid at the free surface is exposed to the ambient temperature. Hence, a cooling condition is applied.

Subsequently, the variable viscosity model is introduced and the equations governing the flow are coupled to this model and solved using both analytical and numerical methods.

VARIABLE VISCOSITY ANALYSIS

Here, the aim of is to analyse a non-Newtonian fluid obeying the Carreau model. The non-dimensional form of the Carreau model is given by:

$$\mu = \left(1 + l \left(\frac{\partial u}{\partial y}\right)^2\right)^{\frac{n-1}{2}}, \quad (15)$$

where $l \approx (\lambda U/H)$. Combining Equations (10) and (15), and integrating with respect to y , and applying the boundary conditions (14) gives,

$$\left(1 + l \left(\frac{\partial u}{\partial y}\right)^2\right)^{\frac{n-1}{2}} \frac{\partial u}{\partial y} = (h - y), \quad (16)$$

for purely gravity driven flow. Equation (16) cannot be solved analytically. However, the case where $l \ll 1$ is considered first to allow for analytical progress. Our interest at this stage is to obtain the maximum upper bound for l . We will use the experimental data for hydroxylethylcellulose solution flowing in a 5 mm thick layer as listed in Table 1 (Myers, 2005; Macosko, 1994; Barnes et al., 1989). The other parameters are given by

given by $\lambda \approx 0.0664$, $\rho g \sin \beta \approx 1000$ and the reference viscosity is given by $\mu_0 = 0.22$. The velocity scale is calculated to be $U = 0.0227$ m/s. Using the aforeseen parameter values we can calculate the value of $l \approx 0.3015$. In the following analysis for $l \ll 1$, we will consider the value of $l = 0.3$ as a maximum upper bound for the approximation of the resulting flow profiles. However, it is important to note that, for different fluids, the maximum upper bound for l will be different. We carry our investigation for hydroxylethylcellulose solution with its maximum upper bound as calculated previously. The asymptotic results are obtained by first considering the values for $l \ll 1$. We further determine the analytical solutions for $n = 0$ representing shear thinning fluids and $n = 2$ for shear thickening fluids. The solutions obtained will be compared with the numerical solution.

Solution for $l \ll 1$

The velocity is now written in a series form,

$$u = u_0 + l u_1, \quad (17)$$

where u_1 is the first order correction term. Substituting Equation (17) into (16) and expanding, leads to,

$$\frac{\partial u_0}{\partial y} + \frac{n-1}{2} l \left(\frac{\partial u_0}{\partial y}\right)^3 + l \left(\frac{\partial u_1}{\partial y}\right) = (h - y). \quad (18)$$

Integrating the leading order terms gives,

$$u_0 = \frac{y}{2}(2h - y). \quad (19)$$

Equation (19) is a standard parabola and can be obtained in several references, (Acheson, 1990; Myers et al., 2006). The l correction terms satisfies,

$$\left(\frac{\partial u_1}{\partial y}\right) + \frac{n-1}{2} \left(\frac{\partial u_0}{\partial y}\right)^3 = 0. \quad (20)$$

Equation (20) corresponds to Equation which can be found in (El Naby et al., 2006). This is solved using the imposed boundary condition $u_1(0) = 0$ to give,

$$u_1 = \frac{(1-n)}{8} [(y - h)^4 - h^4]. \quad (21)$$

To order l the velocity may then be written,

$$u = u_0 + l u_1 = \frac{y}{2}(2h - y) + l \frac{(1-n)}{8} [(y - h)^4 - h^4]. \quad (22)$$

Equations (12) and (15) are coupled to give,

$$\frac{\partial^2 T}{\partial y^2} = -Br \left(\frac{\partial u}{\partial y}\right)^2 \left[1 + l \left(\frac{\partial u}{\partial y}\right)^2\right]^{\frac{n-1}{2}}. \tag{23}$$

Equation (23) must be solved numerically to obtain the full solution. We now follow a similar procedure used to determine the velocity profile to obtain the solution for the temperature profile, that is, the case where $l \ll 1$. Now the temperature can be written in series form,

$$T = T_0 + l T_1, \tag{24}$$

and combining Equations (23) and (24) gives,

$$\frac{\partial^2 T_0}{\partial y^2} + l \frac{\partial^2 T_1}{\partial y^2} = -Br \left[\left(\frac{\partial u_0}{\partial y}\right)^2 + l \frac{(n-1)}{2} \left(\frac{\partial u_0}{\partial y}\right)^4 + 2l \left(\frac{\partial u_0}{\partial y}\right) \left(\frac{\partial u_1}{\partial y}\right) \right]. \tag{25}$$

Integrating the leading order terms with respect to y and applying the boundary conditions (13) yields,

$$T_0 = \frac{Br}{12} \left[h^4 \left(1 - \frac{Bi}{(Bi h - 1)} y\right) - (h - y)^4 \right] + \left(\frac{Bi}{(Bi h - 1)}\right) y. \tag{26}$$

The first order correction terms is,

$$\frac{\partial^2 T_1}{\partial y^2} = -Br \left[\frac{(n-1)}{2} \left(\frac{\partial u_0}{\partial y}\right)^4 + 2 \left(\frac{\partial u_0}{\partial y}\right) \left(\frac{\partial u_1}{\partial y}\right) \right]. \tag{27}$$

Coupling Equations (20) and (27) gives,

$$\begin{aligned} \frac{\partial^2 T_1}{\partial y^2} &= -Br \left[\frac{(n-1)}{2} \left(\frac{\partial u_0}{\partial y}\right)^4 - (n-1) \left(\frac{\partial u_0}{\partial y}\right)^4 \right] \\ &= Br \frac{(1-n)}{2} \left(\frac{\partial u_0}{\partial y}\right)^4. \end{aligned} \tag{28}$$

The boundary conditions for T_1 satisfy,

$$T_1(0) = 0, \left. \frac{\partial T_1}{\partial y} \right|_{y=h} = Bi T_1. \tag{29}$$

The expression for T_1 is therefore,

$$T_1 = \frac{Br(1-n)}{10} \left[(h - y)^6 - h^6 + \left(\frac{Bi}{(Bi h - 1)}\right) y \right]. \tag{30}$$

and so the final temperature profile becomes,

$$\begin{aligned} T &= T_0 + l T_1 \\ &= \frac{Br}{12} \left[h^4 \left(1 - \frac{Bi}{(Bi h - 1)} y\right) - (h - y)^4 \right] + \left(\frac{Bi}{(Bi h - 1)}\right) y \\ &\quad + l \frac{Br(1-n)}{10} \left[(h - y)^6 - h^6 + \left(\frac{Bi}{(Bi h - 1)}\right) y \right]. \end{aligned} \tag{31}$$

Equation (31) provides the solution for the temperature profile. We now proceed to determine the velocity, the flow rate and the temperature profiles when $n = 0$.

Solution for $n = 0$

In order to obtain the solution for the velocity profile for $n = 0$, Equation (16) is now written,

$$\left(1 + l \left(\frac{\partial u}{\partial y}\right)^2\right)^{-\frac{1}{2}} \frac{\partial u}{\partial y} = (h - y). \tag{32}$$

For purely gravity driven flow, Equation (32) gives,

$$\frac{\partial u}{\partial y} = \frac{(h-y)}{\sqrt{(1-l(h-y))^2}}, \tag{33}$$

Note Equation (33) is valid only for $l \ll 1$, this choice of l is reflected in the scaling for U in which gravitational force is the dominant driving force for the flow. Integrating Equation (33) and applying the boundary conditions (13) yields,

$$u = \frac{1}{l} \left[\sqrt{1 - l(h-y)^2} - \sqrt{1 - l h^2} \right]. \tag{34}$$

Equation (34) gives the solution for the velocity profile. To determine the solution for temperature profiles, Equations (12), (15), (32) and (33) are combined to give,

$$\frac{\partial^2 T}{\partial y^2} = -\frac{Br (h-y)^2}{\sqrt{1-l(h-y)^2}}. \tag{35}$$

Integrating Equation (35) and applying the boundary conditions (13) and (14) gives,

$$\begin{aligned} T &= -\frac{Br}{12A} [h^4 - 2y^4 + 5hy^3 - h^3y - 3h^2y^2 - 5h^2 - 2y^2] - \\ &\quad \frac{BrA}{12l} (h^2 - 2y^2) - \frac{Br}{6l^2} (A^{\frac{1}{3}} + A) \\ &\quad - \frac{Br}{12l} \left[hyA + \frac{7hy}{A} + \frac{4}{lA} \right] - \frac{Br h}{l^3} \tan^{-1} \left(\frac{\sqrt{l}(y-h)}{A} \right) (y - \\ &\quad h \\ &\quad - \frac{Br Bi}{12(Bi h - 1)} \left[\left(6h^4 - \frac{5h^2}{l} + \frac{5h}{l} - \frac{6}{l^2}\right) y \right] - \\ &\quad \frac{Bi}{(Bi h - 1)} C_2 y + \frac{Bi}{(Bi h - 1)} y, \end{aligned} \tag{36}$$

Where,

$$\begin{aligned} A &= \sqrt{(1 - l(h - y))^2}, \\ C_2 &= \frac{Br}{12A} [h^4 - 5h^2] + \frac{Br A h^2}{12l} + \frac{Br}{6l^2} (\sqrt[3]{1 - lh} + \sqrt{1 - lh}) \\ &\quad + \frac{Br}{12l^2} \left[\frac{4}{\sqrt{1 - lh}} \right] \\ &\quad + \frac{Br h^2}{l^3} \tan^{-1} \left(\frac{-h\sqrt{l}}{\sqrt{1 - lh}} \right). \end{aligned}$$

Equation (36) gives the solution for the temperature profile. In the following subsection, we proceed to determine the velocity and the temperature profiles for $n = 2$.

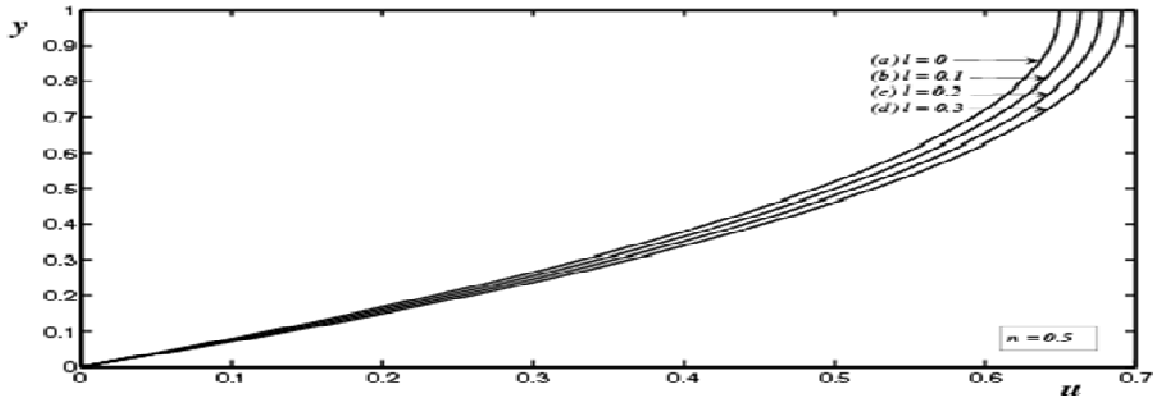


Figure 2. The velocity profiles for Equation (22) with various values of l and $n = 0.5$: Boundary conditions (13) and (14).

Solution for $n = 2$

The velocity profile for the case $n = 2$ is now determined. Equation (16) is written,

$$\left(1 + l \left(\frac{\partial u}{\partial y}\right)^2\right)^{\frac{1}{2}} \frac{\partial u}{\partial y} = (h - y). \tag{37}$$

Equation 37 gives,

$$\left(\frac{\partial u}{\partial y}\right)^2 = \frac{(-1 \pm \sqrt{(1+4l(h-y)^2})}{2l}. \tag{38}$$

For purely gravity driven flow, $(\partial u/\partial y) > 0$. Thus Equation (38) can be expanded to the order $\mathcal{O}(l^2)$ to give,

$$\frac{\partial u}{\partial y} = \frac{1}{2} [2(h - y) - l(h - y)^3]. \tag{39}$$

Integrating Equation (39) and applying the boundary conditions (13) yields,

$$u = \frac{1}{8} [4y(2h - y) + l(h - y)^4]. \tag{40}$$

Equations (12), (38) and (39) are combined and expanded to give,

$$\frac{\partial^2 T}{\partial y^2} = -Br[(h - y)^2 - l(h - y)^4] - \frac{Br l}{2} [(h - y)^2 - l(h - y)^4] \tag{41}$$

Rearranging the terms to the order $\mathcal{O}(l^2)$ in Equation (41), integrating and applying the boundary conditions (13) and (14) gives,

$$T = -\frac{Br}{2} \left[\frac{1}{6} (h - y)^4 - \frac{1}{30} (h - y)^6 \right] - \frac{Bi Br}{2(Bi h - 1)} \left[\frac{h^4}{6} - \frac{l h^6}{30} \right] y + \frac{Br}{2} \left[\frac{h^4}{6} - \frac{l h^6}{30} \right] + \frac{Bi}{(Bi h - 1)} y. \tag{42}$$

Equation (42) gives the solution for the temperature profile when $n = 2$.

The presentation of the results is organised as follows. The effect of l when $n = 0$ and $n = 2$ on the resulting flow profiles is also investigated. Note that in the limit as $l \rightarrow 0$, the Newtonian results is recovered as expected, for the $n = 0$ case.

The velocity profiles corresponding to Equation (22) are plotted in Figure 2 with $n = 0.5$ and Figure 3 with $n = 1.5$ respectively. The figures plotted have different values of l and the film height is fixed at $h = 1$. In Figure 2, for $l = 0$, the Newtonian velocity profile is retrieved in curve (a). When l increases the viscosity of the fluid decreases for shear thinning fluids and the velocity increases as the resistance force to the flow decreases with its maximum occurring at the top layer. In Figure 3, with $n \geq 1.5$, the curves illustrate that when l decreases the velocity of the fluid decreases. When the parameter l decreases the fluid viscosity decreases for shear thickening fluids and the velocity increases accordingly. This shows that the less viscous is the fluid the higher the flow.

Figures 4 and 5 shows the temperature profiles for Equation (31). The temperature profiles are plotted with different values of $l, n = 0.5$ and $n = 1.5$. The other parameters are given by $Bi = 0.3$ and $Br = 0.3$ for all these figures. In each figure the temperature profiles are plotted with different values of l similar to those used in Figure 2 with $n = 0.5$ and Figure 3 with $n = 1.5$ respectively.

In Figure 4 the fluid temperature increases when the non-dimensional parameter l increases, for shear thinning fluids. This shows that heat generation as a result of the viscous term is high when l increases. In Figure 5 the temperature of the fluid for shear thickening fluids is contrary to the curves displayed in Figure 4. The temperature of the fluid increases when l decreases. Heat generation by the viscous term in curves (a) to (d) is higher when the parameter l decreases.

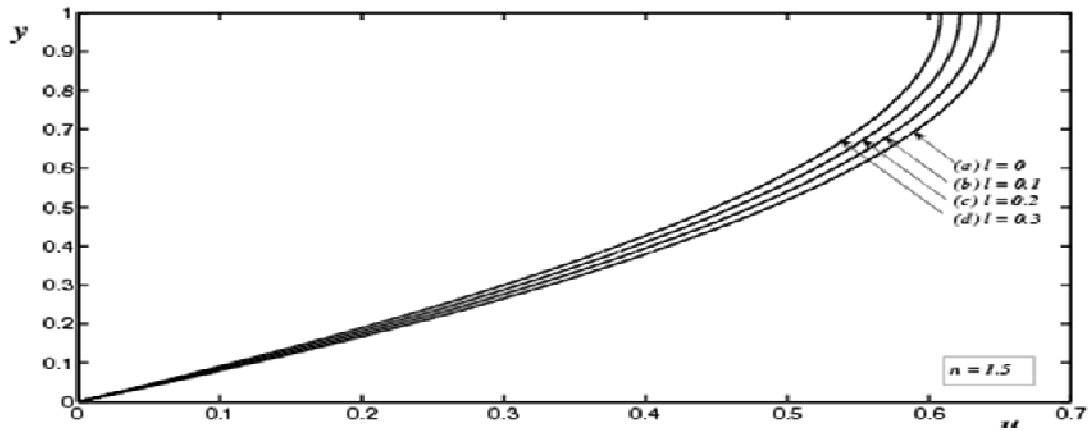


Figure 3. The velocity profiles for Equation (22) with various values of l and $n = 1.5$: Boundary conditions (13) and (14).

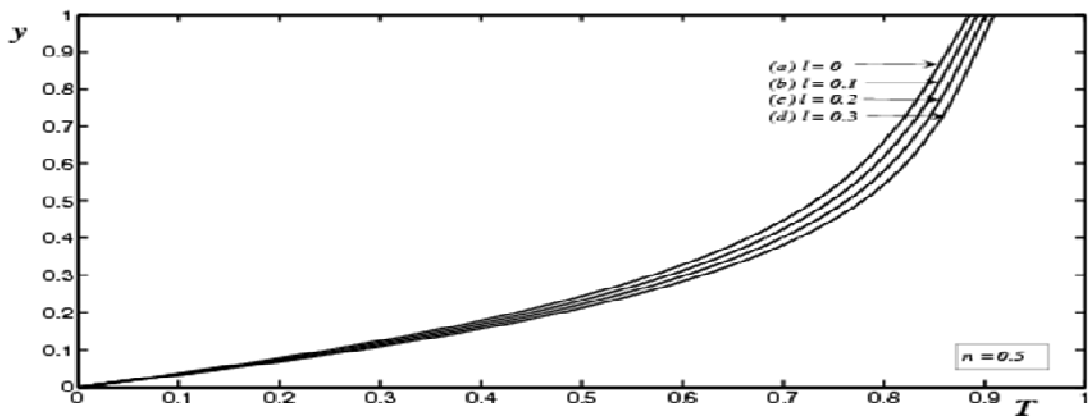


Figure 4. The temperature profiles for Equation (31) with various values of l and $n = 0.5$: Boundary conditions (13) and (14).

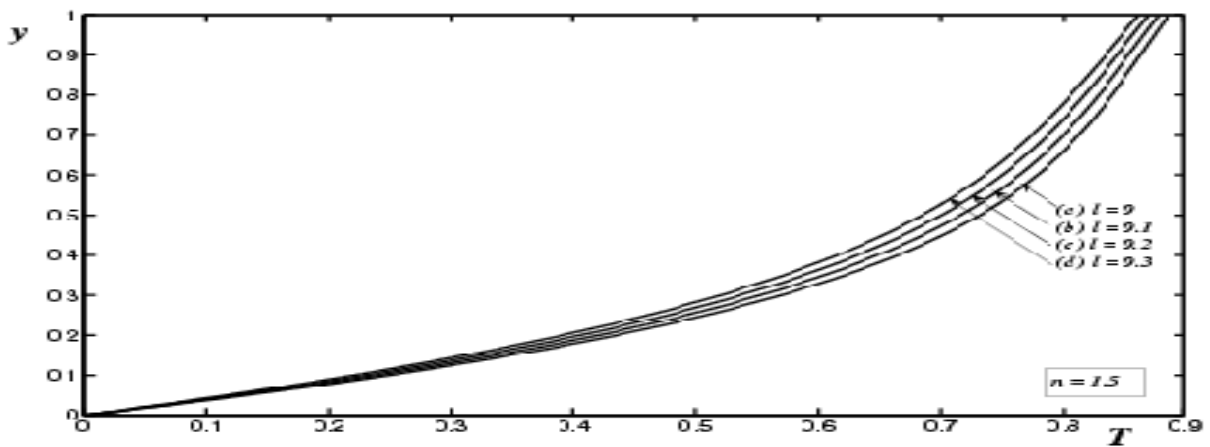


Figure 5. The temperature profiles for Equation (31) with various values of l and $n = 1.5$: Boundary conditions (13) and (14).

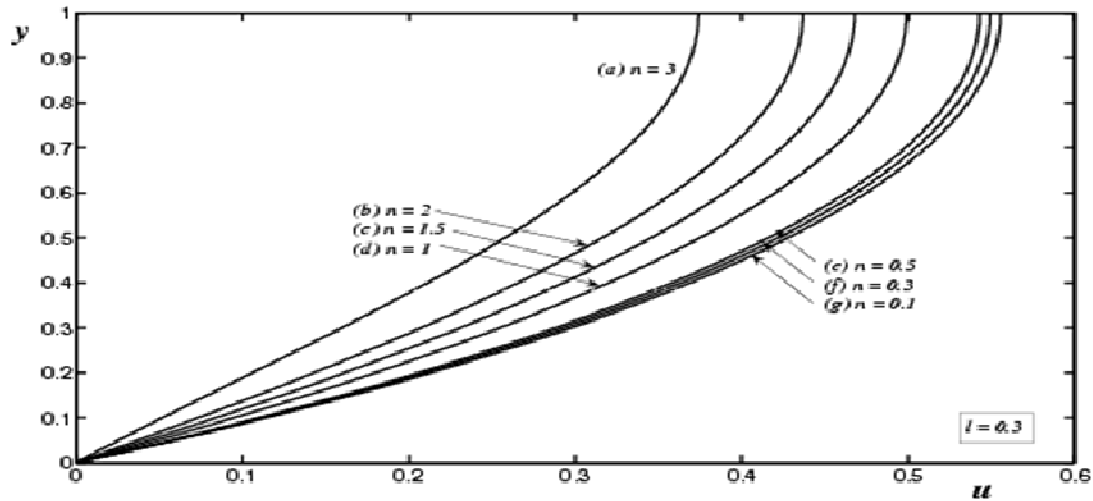


Figure 6. The velocity profiles corresponding to Equation (22) with $l = 0.3$: Boundary conditions (13) and (14).

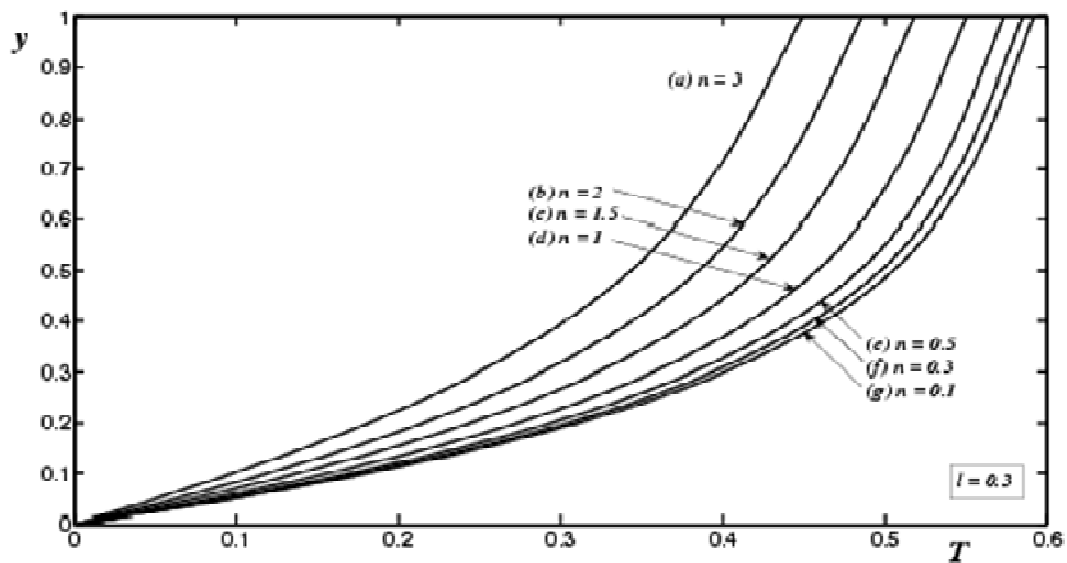


Figure 7. The temperature profiles corresponding to Equation (31) with $l = 0.3$: Boundary conditions (13) and (14).

The velocity profiles are now investigated for various power law indices. Equation (22) is plotted for several values of n between $0.1 \leq n \leq 3$ and $l = 0.3$, in Figure 6. The figure shows that when n decreases, the velocity of the fluid increases across the layer to their maximum values at the free surface. For $n < 1$, the velocity of the fluid increases gradually whilst for $n > 1$ the gap between the fluid velocity is more pronounced with the maximum value for the velocity profile in curve (g) approximately half of the maximum value for the velocity in curve (a). It

is shown in this figure that when $n < 1$, the resistance force to the flow for shear thinning fluids is less as n decreases, and the fluid velocity increases significantly. In Figure 7 the temperature profiles corresponding to Equation (31) are plotted for the same parameter values as in Figure 6, the Brinkman number is fixed at $Br = 0.3$ and the Biot number is also fixed at $Bi = 0.3$. All these curves are similar in shape and the fluid temperature increases to their maximum temperatures at the top layer. In this case when $n < 1$ again we observe the fluid

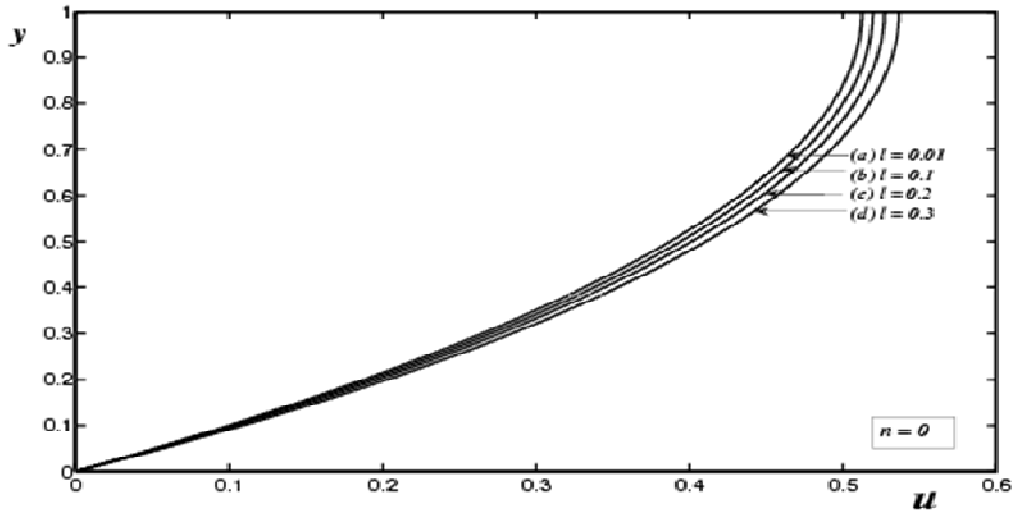


Figure 8. The velocity profiles corresponding to Equation (34) with different values of l and $n = 0$: Boundary conditions (13) and (14).

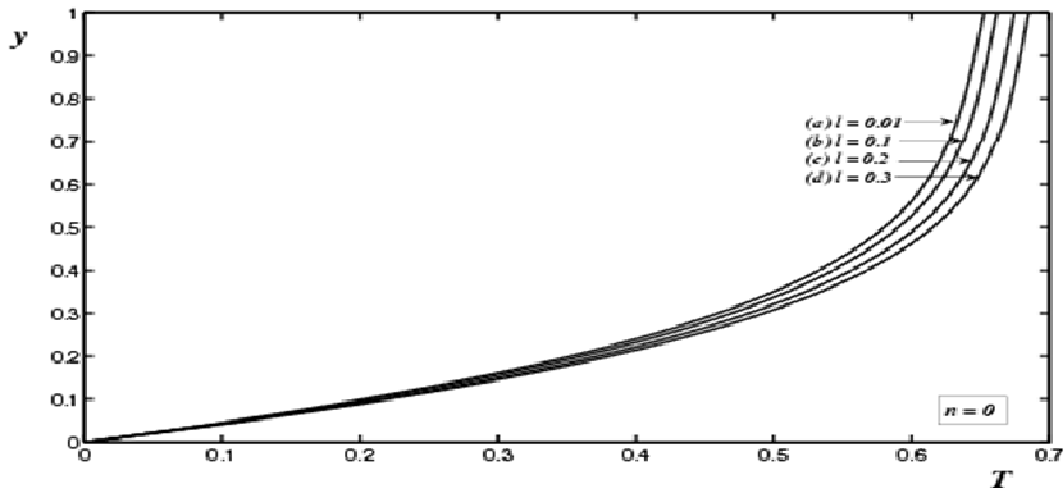


Figure 9. The temperature profiles corresponding to Equation (36) with different values of l and $n = 0$: Boundary conditions (13) and (14).

temperature increasing gradually and for $n > 1$ the gap between the temperature profiles is more pronounced and the fluid temperature increases as n decreases. This figure illustrates that the temperature of the fluid increases due to viscous heat generation.

The velocity profiles corresponding to Equation (34) are now plotted for different values of l with $n = 0$. In Figure 8 curves (a) to (d) are shown and the velocity of the fluid increases and the gap between them is approximately 2%. The viscosity of the fluid decreases when l increases and subsequently an increase in the fluid velocity is observed due to less resistance force to the flow. In

Figure 9 the temperature profiles resulting from Equation (36) are shown. The Brinkman and the Biot numbers are fixed at $Br = Bi = 0.3$ and the values of l are the same as those which are shown in Figure 8. In Figure 9 when l increases, the temperature of the fluid increases and the maximum values for these profiles occur at the free surface and the gap between the profiles is again 2%. This figure illustrates that the temperature of the fluid increases as l increases due to heat generation by the internal flow processes such as viscous action, which acts to increase the temperature of the fluid.

The velocity profiles corresponding to Equation (40) are

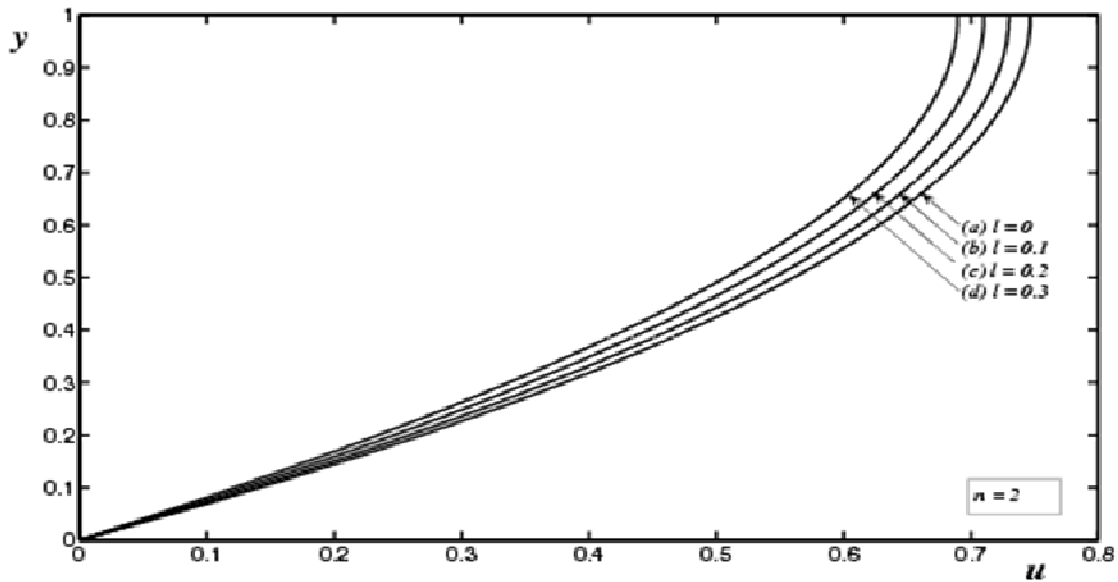


Figure 10. The velocity profiles corresponding to Equation (40) with different values of l and $n = 2$: Boundary conditions (13) and (14).

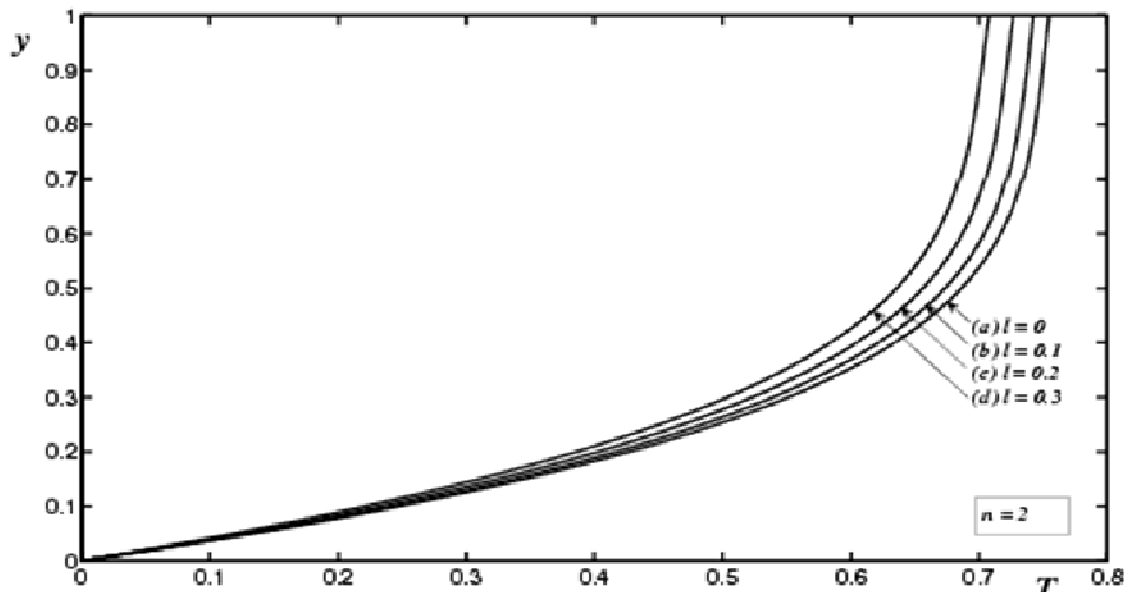


Figure 11. The temperature profiles corresponding to Equation (42) with different values of l and $n = 2$: Boundary conditions (13) and (14).

shown in Figure 10 with different values of l and $n = 2$. In this figure the fluid behaviour shows the opposite of the curves as displayed in Figure 8. In curves (a) to (d) the velocity of the fluid increases when the values of l decreases. These curves demonstrate that when l decreases, the velocity increases across the layer, since

the viscosity is decreasing and the resistance force to the flow decreases resulting in an increase in the velocity of the fluid. In Figure 11 the temperature profiles corresponding to Equation (42) are displayed with $Br = Bi = 0.3$ and different values of l as shown in the figure. In this figure again we observe the complete

opposite behaviour of shear thinning fluids in Figure 9. In Figure 11 when l decreases, the temperature of the fluid increases. The increase in the fluid temperature is caused by the viscous heat generation, which also act to raise the temperature of the fluid in the layer.

Subsequently, the velocity and the temperature profiles will be investigated using a numerical method and considering large values of a non-dimensional parameter l . We again investigate the effect of the power law index on the resulting flow profiles.

NUMERICAL SCHEME FOR THE CARREAU MODEL

In variable viscosity analysis discussed previously, the analytical results were obtained for values of $l \ll 1$, $n = 0$ and $n = 2$. A numerical solution valid for all values of l is now introduced. The Newton Raphson method is used to obtain a full solution for the velocity and temperature profiles, (Borse, 1999; Burden et al., 2001). Numerical results are compared with analytical results obtained in the previous section for $l \ll 1$, $n = 0$ and $n = 2$. The analytical results are used as a benchmark to validate the numerical code. Equations (16) and (23) may be written,

$$\left(\frac{\partial u}{\partial y}\right)^{\frac{2}{n-1}} + l \left(\frac{\partial u}{\partial y}\right)^{\frac{24}{n-1}} - (h - y)^{\frac{2}{n-1}} = 0 \quad (43)$$

$$\frac{\partial^2 T}{\partial y^2} + Br \left(\frac{\partial u}{\partial y}\right)^2 \left[1 + l \left(\frac{\partial u}{\partial y}\right)^2\right]^{\frac{n-1}{2}} = 0 \quad (44)$$

The coupled, non-linear partial differential Equations (43) and (44) are now solved numerically to obtain a full solution for the velocity u and temperature T . The fluid dept is divided into two j cells of step size Δy . The values of u and T in the i^{th} cell are denoted by u_i and T_i respectively.

Equation 43 takes the form,

$$\left(\frac{\partial u}{\partial y}\right)^{\frac{2}{n-1}} \Big|_{y=y_i} + l \left(\frac{\partial u}{\partial y}\right)^{\frac{24}{n-1}} \Big|_{y=y_i} = (h - y_i)^{\frac{2}{n-1}}, \quad (45)$$

where $y_i = i\Delta y$ and Δy denote the step size between the cells. The space derivative is calculated using Newton's algorithm in every cell. In this case an initial approximation of u_0 and T_0 is generated in order to obtain the next approximation value.

The boundary conditions give the initial iteration, that is, $u_0 = 0$ at $y = 0$ and $T_0 = 0$ at $y = 0$. We solve for $(\partial u / \partial y)$ and then calculated u throughout the layer, and the velocity may be calculated using the standard integration method,

$$u_{i+1} = u_i + \Delta u_y \cdot \frac{\partial u}{\partial y} \Big|_{y=y_i}, \quad (46)$$

at $y = y_i$. Finally, Equation (44) is integrated twice to give the full solution for the temperature profile. The results are now plotted for various values of l and n .

We begin our discussion of the numerics by first comparing the analytical solution with a full solution obtained using a numerical code. We use MATLAB to derive the full solution from the governing equations using the Newton Raphson numerical method. We first test our numerical code by comparing the solution resulting from Equations (44) and (45) with $n = 0$ for shear thinning fluids and $n = 2$ for shear thickening fluids. The velocity profiles are plotted from Equations (22), (34), (40) and (45) for comparison purposes. The temperature profiles are also plotted for Equations (31), (36), (43) and (44) respectively. For the sake of simplicity, we first compare our numerical code using two small values for the non-dimensional parameter l , namely $l = 0.1$ and 0.3 . If the analytical results are in agreement with the numerics, we proceed to investigate the numerics for large values of l . We proceed again to investigate the behaviour of shear thinning fluids and shear thickening fluids for large values of l . The effect of the power law index n on the velocity and temperature profiles is again investigated using the solution obtained numerically.

In Figure 12 the velocity profiles corresponding to Equations (22), (34) and (45) are plotted in curves (a) and (b). In this case the power law index is given by $n = 0$ and $l = 0.1$ and 0.3 as shown in both sets of curves. In set (a), the dash line represents the solution of Equation (22), the solid line is from the numerics in Equation (45) and the dash dot line represents the plots for Equation (34). In set (a) all the curves compare closely and in set (b) all the curves shows a good agreement. Curves (c) to (f) represents the numerical solutions with large values of l , namely $l = 1, 3, 7$ and 10 . We observe that increasing the values of l results in a significant increase in the fluid velocities. The viscosity of the fluid decreases when l increases, then the fluid velocity increases significantly since the resistance force to flow is diminishing. The convergence of our numerical scheme is obtained within the region $1 \times 10^{-7} < \Delta y < 1 \times 10^{-9}$. In this range our numerical results do not accept any further grid refinements or changes. The opposite of this behaviour in the velocity of the fluid is shown in Figure 13 with $n = 2$ for shear thickening fluids. The dash dot line is plotted from Equation (40) and the other curves are as explained above. This figure illustrate that when l decreases the velocity of the fluid increases as expected from shear thickening fluid, due to decreasing resistance force to the flow. In this figure the numerical solution compares well with the analytical solution as shown in curves (e) and (f) for $l = 0.1$ and $l = 0.3$ respectively.

The comparison for the temperature profiles is shown in Figure 14 with $n = 0$ for shear thinning fluids and Figure 15 with $n = 2$ for shear thickening fluids. Figure 14 shows curves corresponding to Equations (31), (36) and

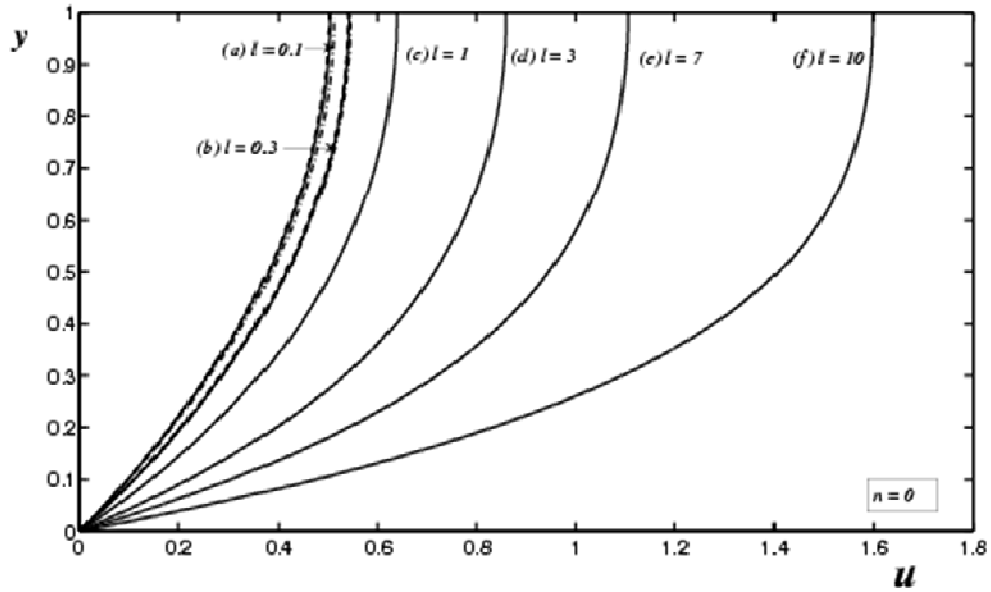


Figure 12. The velocity profiles corresponding to Equations (22), (34) and (45) with different values of l : Boundary conditions (13) and (14).

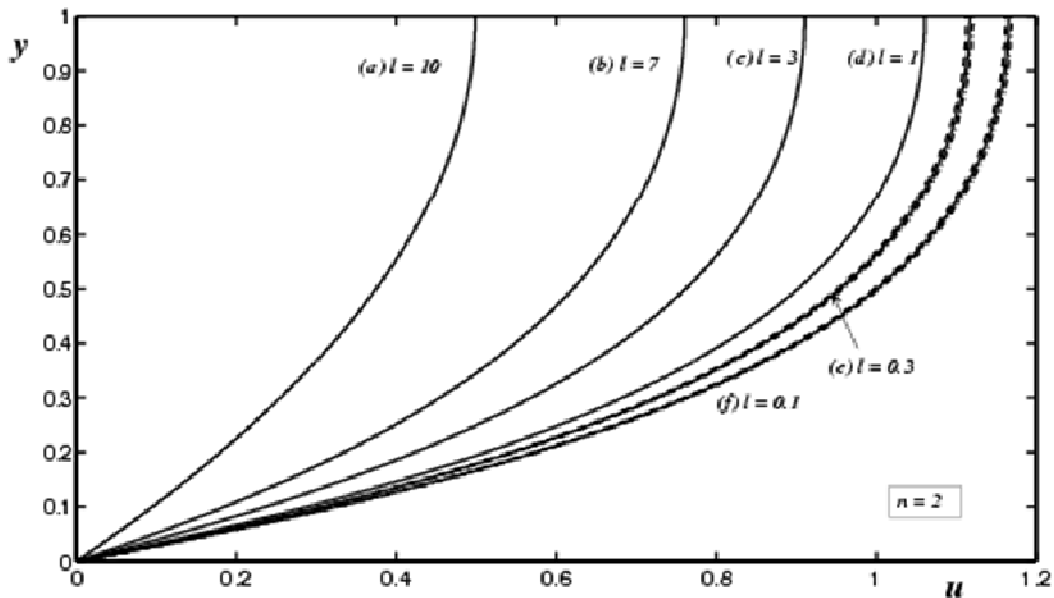


Figure 13. The velocity profiles corresponding to Equations (22), (40) and (45) with different values of l : Boundary conditions (13) and (14).

(44) with $n = 0$, $Br = Bi = 0.3$ and different values of l as displayed in the figure. For the set of curves (a), the dash line represents the solution for Equation (31), the solid line is from the numerics in Equation (44) and the dash dot line represents the solution for Equation (36). In (b) we again observe that the three curves compare well with the numerics. Curves (c) to (f) show the numerical

solution for increasing temperature of the fluid when l increases. The numerical solutions displayed in these curves show maximum temperatures which are greater than the asymptotics as shown previously, since large values for l are considered for the numerical method. Heat is generated in the layer as a result of the action of a viscous force, which causes the collision amongst the

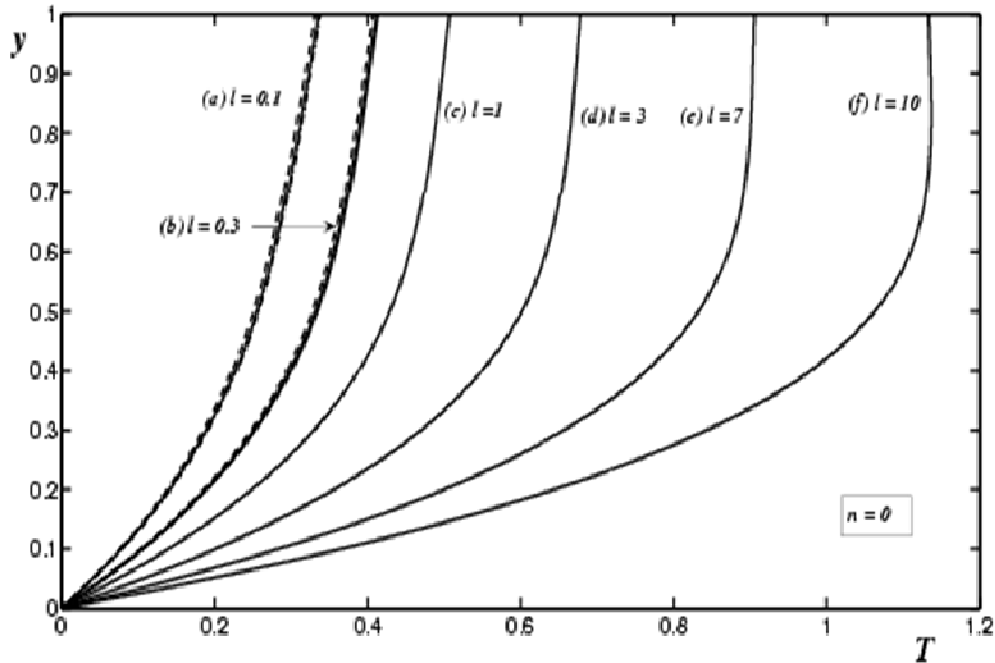


Figure 14. The temperature profiles corresponding to Equations (31), (36) and (44) with different l : Boundary conditions (13) and (14).

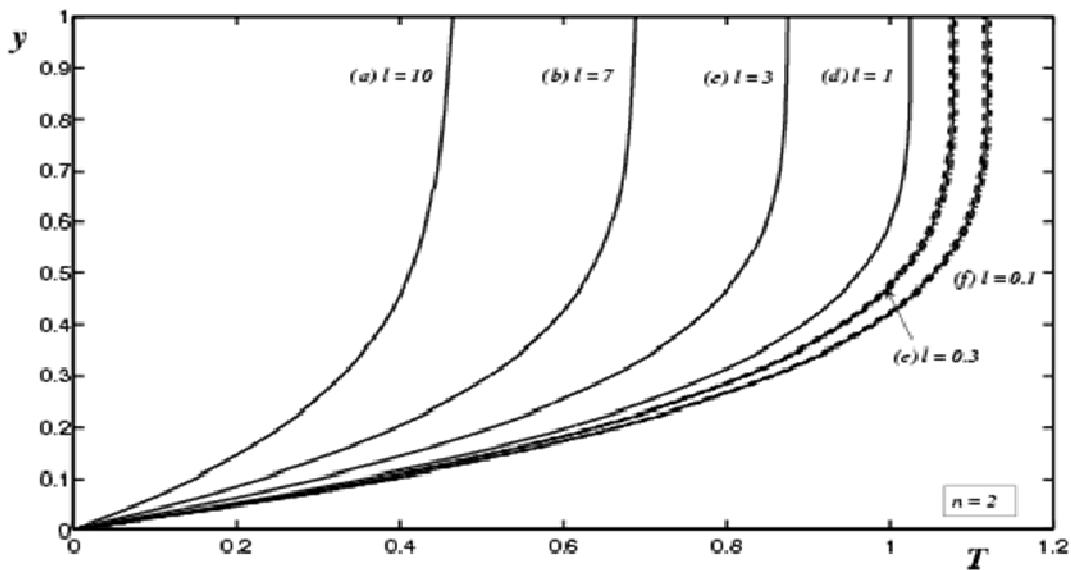


Figure 15. The temperature profiles corresponding to Equations (31), (42) and (44) with different values of l : Boundary conditions (13) and (14).

fluid molecules and subsequently the temperature of the fluid increases. The opposite of this behaviour of the temperature profiles in Figure 14 is shown in Figure 15. In Figure 15 the dash dot line is plotted from Equation (42). The temperature increases as the non-dimensional

parameter l decreases, with the maximum values for the Newtonian case much higher than for the non-Newtonian fluid with $l = 10$. We again observe that the temperature profiles plotted from the numerics are also in agreement with the analytical solution.

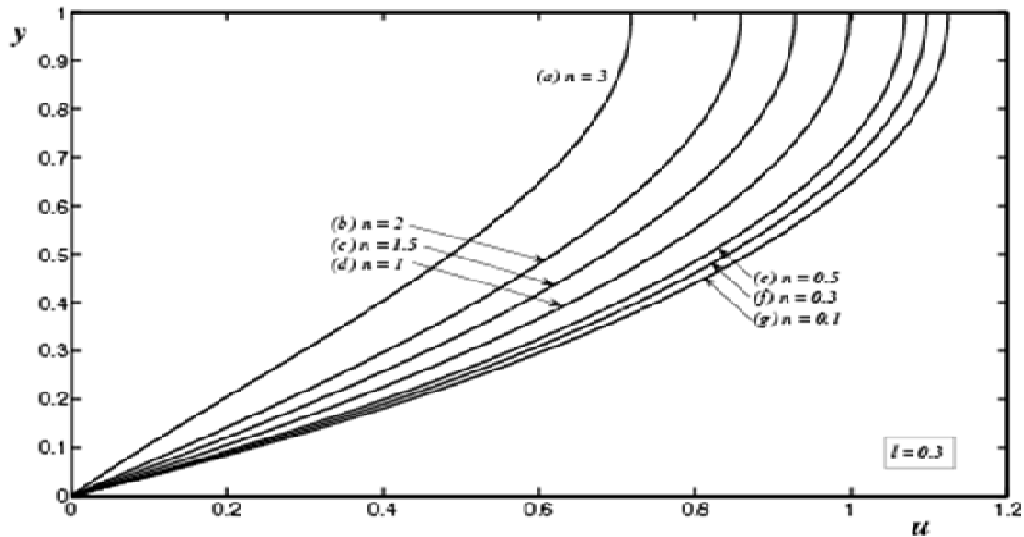


Figure 16. The velocity profiles corresponding to Equation (45) with different values of n and $l = 0.3$: Boundary conditions (13) and (14).

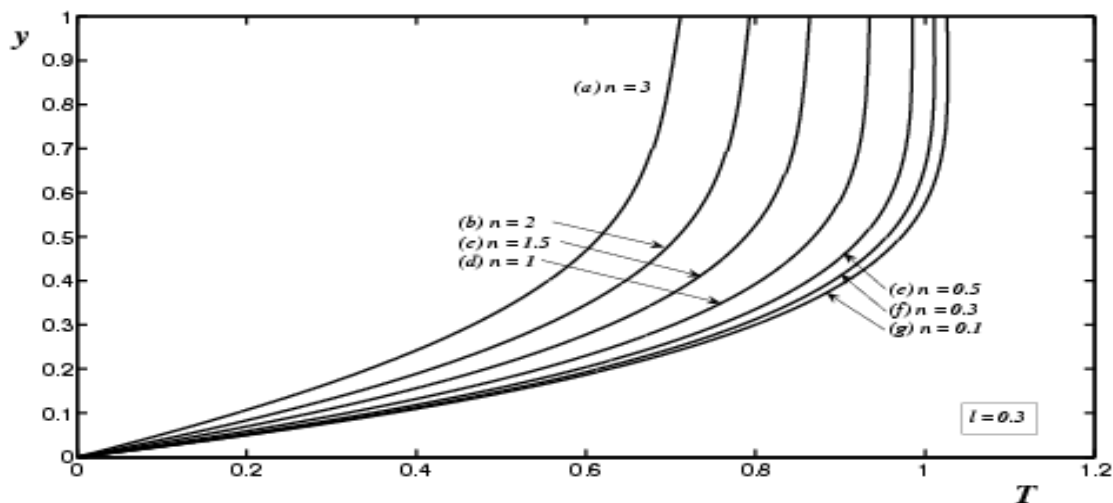


Figure 17. The temperature profiles corresponding to Equation (44) with different values of n and $l = 0.3$: Boundary conditions (13) and (14).

Figure 16 shows the numerical velocity profiles for various values of the power law index n with $l = 0.3$. The fluid velocity for all seven curves increases nonlinearly across the layer to their maximum velocities at the free surface. The result show that the gap between the velocity profiles when n is in the region 0.1 and 0.5 is small and when n is in the region 1 to 3 the gap between the velocity profiles is more pronounced. We observe that the fluid velocity increases when n decreases as a result of the decreasing resistance force to the flow. The Newtonian velocity profile is retrieved in curve (d) with $n = 1$. The velocity profiles resulting from the Carreau

model are in agreement with the results shown in (Myers, 2005), for shear thinning fluids. However, our velocity profiles show significantly higher maximum values as compared to the profiles in Myers (2005), probably due to high shear rates involved in the materials which were investigated. Akyildiz et al. (2007), used the Runge Kutta method to solve for the velocity profiles for a shear thinning fluid with $n = 0.25$ and the Newtonian fluid with power law index $n = 1$, which is in agreement with our results. Their results revealed that the velocity profile for $n = 0.25$ is slightly higher than the Newtonian case. In Figure 17 the temperature profiles are plotted for the

same parameter values of the power law index as shown in Figure 16 with $l = 0.3$ and $Br = Bi = 0.3$. All these temperature curves are similar in shape and the fluid temperatures increase to their maximum levels at the top layer. This shows that the viscous term acts to increase heat generation in the fluid and the temperature of the fluid rises. In the case where $n = 0.1$ and $n = 0.5$, the temperature of the fluid increases gradually as shown in curves (e) to (g), however, in curves (a) through to (d) the gap between the temperature profiles is more pronounced.

Conclusion

In conclusion, the effect of the flow controlling parameters on the resulting velocity and temperature profiles, were obtained using an analytical and numerical technique. The velocity and temperature profiles increase when the power law index n decreases. The results were extended to include a full solution using the Newton Raphson numerical method for larger values of l . The velocity and temperature profiles for small values of l and $n = 0$ were compared and the curves for these profiles are in agreement in particular when $l = 0.3$. Similarly, the results for the velocity and temperature profiles were compared for various values of l with $n = 2$. The results showed good agreement between the analytical results and the numerics, particularly when $l = 0.3$. Therefore, the effect of large values of l on the resulting flow profiles is investigated. The resulting flow profiles shows that the velocity and temperature of the fluid increases significantly when l increases with the power law index $n < 1$ and the opposite is true for $n > 1$. The effect of the power law index n on the resulting flow profiles showed that as n decreases, both the velocity and the temperature of the fluid increases. The numerical solution is preferable since it can be used for larger values of l but the asymptotic solution is useful as a benchmark.

REFERENCES

- Acheson DJ (1990). Elementary Fluid Dynamics. Oxford Uni. Press.
- Akyildiz FT, Vajravelu K (2007). Orthogonal cubic spline collocation method for the nonlinear parabolic equation arising in a non-Newtonian flow. Appl. Math. Comput., 189:462-471.
- Alhama F, Zueco J (2007). Application of a lumped model to solids with linearly temperature dependent thermal conductivity. Appl. Math. Modelling, 31:302-310.
- Bair S (2006). A Reynolds-Ellis equation for line contact with shear thinning. Tribology Int. Elsevier Ltd., 39:310-316.
- Barnes HA, Hutton JF, Walters F (1989). An Introduction to Rheology. B. V.
- Borse GJ (1997). Numerical Methods with MATLAB. PWS Publishing Co.
- Burden RL, Faires JD (2001). Numerical Analysis, 7th edition. Thompson Learning.
- Constantinescu VN (1995). Laminar Viscous Flow. Springer-Verlag.
- Eastop TD, McConkey A (1978). Applied Thermodynamics for Engineering Technologists, 3rd edition. Longman Group, Ltd.
- El Naby AE, El Misery EEM, El Kareem MFA (2006). Effects of a magnetic field on trapping through peristaltic motion for generalized Newtonian fluid in channel. Physica A, 367:79-92.
- Feng J, Leal LG (1999). Pressure driven channel flows of a model liquid-crystalline polymer. Phys. Fluids., 11(10):2821-2835, 1999.
- Fomin S, Hashida T, Watterson J (2003). Fundamentals of steady state non-Newtonian rimming flow. J. non-Newtonian Fluid Mech., 111:19-40.
- Haldenwang R, Slatter P, Chhabra R (2004). The thin film approximation for laminar flow in open channels for non-Newtonian fluids. 9th Int. Seminar on Paste and Thickened Tailings, Cape Town, South Africa, 31 March - 2 April.
- Holman JP (1990). Heat Transfer, 6th edition. McGraw-Hill, Inc.
- Khaled ARA (2008). Conduction heat and entropy transfer in a semi infinite medium and wall with a combined periodic heat flux and convective boundary condition. Int. J. Thermal Sci., 47:76-83.
- Macosko CW, (1994). Rheology, Principles, Measurements, and Applications. VCH., Inc.
- Makinde OD (2010). Thermodynamic second law analysis for a gravity driven variable viscosity liquid film along an inclined heated plate with convective cooling. J. Mech. Sci. Technol., 24 (4), 899-908.
- Makinde OD (2006). Laminar falling liquid film with variable viscosity along an inclined heated plate. Appl. Math. Computat., 175, 80-88.
- Myers TG (2005). Application of non-Newtonian models to thin film flow. Phy. Rev. E., 72(1):1-11.
- Myers TG, Charpin JPF, Tshehla MS (2006). The flow of a variable viscosity fluid between parallel plates with shear heating. Appl. Math. Modelling, 30:799-815.
- Rouser F, Millet S, Botton V, Hadid B (2007). Temporary stability of Carreau fluid flow down an incline. J. Fluids Eng., 129:913-939.
- Schetz JA, Fuhs AE (1999). Fundamentals of Fluid Mechanics. John Wiley & Sons, Inc.
- White FM (1994). Fluid Mechanics, 3rd edition. McGraw-Hill, Inc.